

Conversion of CO₂-Derived Amorphous Carbon into Flash Graphene Additives

Paul Andrade Advincula, Wei Meng, Jacob L. Beckham, Satish Nagarajaiah, and James M. Tour*

CO₂ emissions have become a significant environmental problem over the last few decades, often stemming from combustion of fossil fuels. Production and disposal of waste plastic also contribute greatly to greenhouse gas emissions, due to combustion of fossil fuels during manufacture and incineration or pyrolysis of the waste materials. Hence, researchers have begun developing technologies geared toward the capture, sequestration, and utilization of CO₂. Several methods are shown to be useful for conversion of gaseous CO₂ into solid carbon feedstocks, such as molten carbonate electrolysis. At the same time, flash Joule heating can rapidly and inexpensively convert carbon-rich feedstocks into flash graphene (FG). Here, amorphous carbon derived from molten carbonate electrolysis of carbon dioxide is converted into FG, sometimes in combination with waste plastic, and demonstrated for use as a reinforcing additive in composite applications. FG can be used in epoxy and vinyl ester resins with a maximum increase in Young's modulus and hardness of 73% and 73%, respectively. Life cycle assessment also shows that adding 5 wt% 25:75 amorphous carbon-derived FG to the epoxy results in 7.7%, 5%, and 2.7% decreases in CO₂ emissions, water consumption, and energy consumption, respectively.

supplied by fossil fuels.^[2] Combustion of these fuels has led to a rapid increase in greenhouse gas emissions, specifically that of carbon dioxide (CO₂).^[3] CO₂ is the most common gas emitted from anthropogenic processes. Certain processes, such as the Haber–Bosch process, convert hydrogen and nitrogen into ammonia, but at a very high CO₂ emission rate.^[4] As such, there is significant interest in technologies that can fix CO₂, particularly methods that can generate useful solid materials from that CO₂-derived carbon.

Several processes have been explored for conversion of CO₂ into solid carbon, such as reaction of CO₂ with LiAlH₄,^[5] chemical vapor deposition,^[6] or molten carbonate electrolysis.^[7] Molten carbonate electrolysis has been successful for the conversion of CO₂ into a variety of nanomaterials, including graphite, carbon nanotubes,^[8] and carbon nano-onions.^[9] The high cost of carbon nanotubes (>\$100 000 per ton)^[10] and graphene (\$60 000–200 000 per ton)^[11] further incentivizes the conversion of CO₂ into carbon nanomaterials.

1. Introduction

Despite growth in large-scale renewable energy solutions, fossil fuels will likely remain the primary energy source for the next few decades.^[1] 85% of the energy used for industrial activities is


Graphene is one of the most promising types of carbon nanomaterials, due to its unique, honeycomb structure of carbon atoms. The graphene structure imparts outstanding mechanical,

P. A. Advincula, J. L. Beckham, J. M. Tour
Department of Chemistry
Rice University
6100 Main Street, Houston, TX 77005, USA
E-mail: tour@rice.edu

W. Meng, S. Nagarajaiah
Department of Civil and Environmental Engineering
Rice University
6100 Main Street, Houston, TX 77005, USA

S. Nagarajaiah
Department of Mechanical Engineering
Rice University
6100 Main Street, Houston, TX 77005, USA

S. Nagarajaiah, J. M. Tour
Smalley-Curl Institute, NanoCarbon Center, and the Rice Advanced Materials Institute
Rice University
6100 Main Street, Houston, TX 77005, USA
S. Nagarajaiah, J. M. Tour
Department of Materials Science and Nano Engineering
Rice University
6100 Main Street, Houston, TX 77005, USA

 The ORCID identification number(s) for the author(s) of this article can be found under <https://doi.org/10.1002/mame.202300266>

© 2023 The Authors. Macromolecular Materials and Engineering published by Wiley-VCH GmbH. This is an open access article under the terms of the Creative Commons Attribution License, which permits use, distribution and reproduction in any medium, provided the original work is properly cited.

DOI: 10.1002/mame.202300266

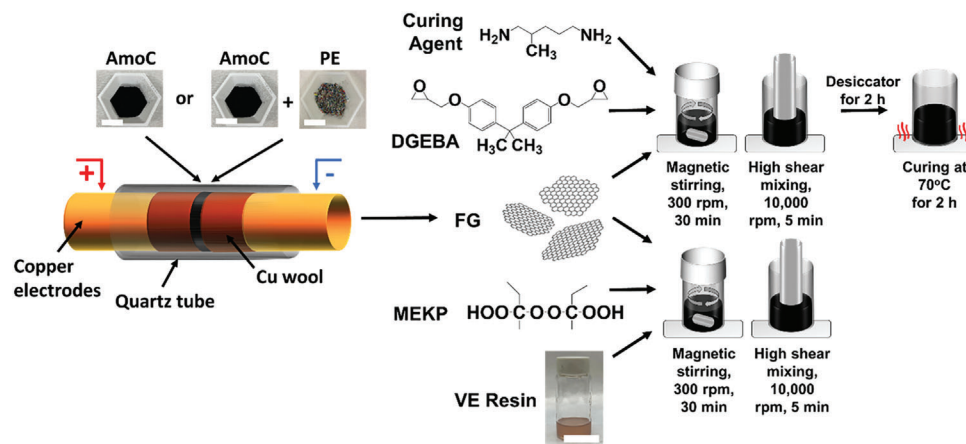


Figure 1. Schematic depicting FJH of AmoC and AmoC:PE blends into FG for use as reinforcing additives in VE and DGEBA composites. Scale bars on images of AmoC, PE, and VE resin are 2.5 cm.

thermal, and electrical properties. These properties make graphene extremely attractive for applications in energy storage and composites. A variety of techniques for making graphene are available, including chemical vapor deposition and liquid phase exfoliation of graphite, but these techniques are generally energy- or chemically intensive.^[12]

Our group recently developed a technique for graphene synthesis involving rapid, solvent- and water-free Joule heating.^[13] Carbon-containing feedstocks are compressed between electrodes and an electrical current is passed through the sample. This causes the sample to heat to >3000 K in milliseconds, breaking carbon-carbon bonds and enabling the atoms to rearrange into the more thermodynamically stable form of graphene. Most non-carbon elements are sublimed out during this process. The resulting “flash” graphene (FG) is turbostratic^[14] and less defective than graphene made by the reduction of graphene oxide.^[15] flash Joule heating (FJH) enables rapid, inexpensive graphene synthesis from any carbon-containing feedstock, including rubber tires,^[16] metallurgical coke,^[17,18] asphaltene,^[19] and carbon black.^[20–22]

In addition to CO₂ emission concerns, plastic pollution is also a significant environmental problem.^[23] Production of plastic requires emissive processes that will account of 1125 megatons of CO₂ and 20% of total oil consumption by the year 2050.^[24,25] After use, the plastic poses an environmental hazard, due to landfilling or incineration of the waste plastic. This waste plastic can have significant impacts on humans^[26,27] and marine life,^[28,29] threatening global oxygen supplies.^[30,31] Due to these environmental hazards, researchers are continually searching for applications or solutions for ever-increasing amounts of plastic waste.

In this work, amorphous carbon (AmoC) derived from CO₂ through molten carbonate electrolysis is converted into flash graphene (FG) through the FJH method. Production of 1 kg of Saratoga Energy AmoC consumes 3.76 kg of CO₂ and 40 kWh of energy. As such, conversion of CO₂ into AmoC and FJH of AmoC into FG is a carbon-negative process that produces FG that can act as a reinforcing additive in epoxy composites. The emissions associated with the final composite can be reduced during production of the reinforcing additive and by reducing the amount of composite required for a given application. AmoC is also blended

with waste polyethylene (PE) to demonstrate its feasibility to act as a carbon-negative conductive additive for upcycling of waste plastics. By using FJH to convert AmoC and AmoC:PE, FG can be made rapidly and inexpensively, without use of solvents or chemical post-processing. The resulting FG materials are then used as effective, carbon negative reinforcing additives in vinyl ester and epoxy composites.

2. Results and Discussion

AmoC and blends of AmoC:PE are FJH into FG, as shown in **Figure 1**. The resulting FG materials are combined with VE or diglycidyl ether bisphenol A (DGEBA) resin in a 20 mL scintillation vial and stirred with a magnetic stir bar. To enhance the dispersion and shearing of the FG within the matrix material, high shear mixing is then used. Finally, methyl ethyl ketone peroxide (MEKP) hardener is added to the VE solution and the entire solution is allowed to cure overnight. When making DGEBA composites, an additional degassing step and heating step are used. Due to the consumption of CO₂ in the production of AmoC, this results in a carbon-negative reinforcing additive that can be added to VE or DGEBA to improve their mechanical properties, as well as to reduce CO₂ emissions, water consumption, and energy consumption.

Raman spectroscopy is a powerful tool for characterization of carbon and graphene materials. Quality of graphene can be assessed by analyzing the intensity ratios of three different peaks that regularly appear in graphene: D (≈1350 cm⁻¹), G (≈1580 cm⁻¹), and 2D (≈2700 cm⁻¹). The D band appears when defects and graphene edges are present, with increasing intensity as the concentrations of these features increase. The G band appears in response to a commonly observed in-plane phonon mode in graphitic carbon. Finally, the 2D band arises from the overtone of the in-plane transverse optic branch. A lower I_D/I_G ratio is generally desirable, as this indicates a lower concentration of defects and a higher I_{2D}/I_G ratio is generally desirable, as this indicates that fewer graphene layers are present, thereby facilitating dispersion in the resins.

The average Raman spectrum of the AmoC has a very high I_D/I_G and very low I_{2D}/I_G ratio, indicating that this material is

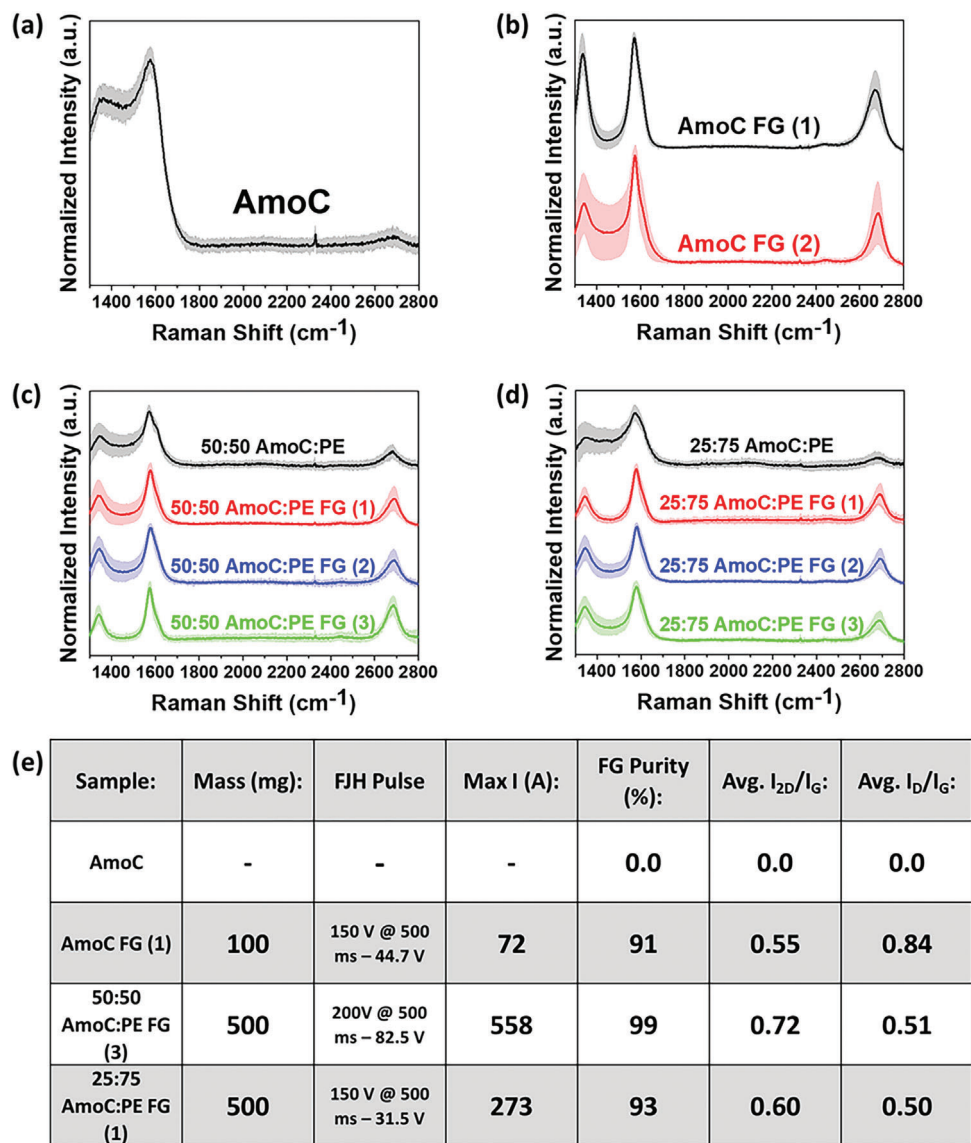


Figure 2. Average Raman spectroscopy curves for a) AmoC and all conditions for FJH of b) AmoC FG, c) 50:50 AmoC:PE FG, and d) 25:75 AmoC:PE FG. Different voltages are applied to each material during optimization, as denoted by the different colors and numbers, for example, AmoC FG (1) versus AmoC FG (2). Standard deviation is shown by the shaded areas ($N = 100$). e) Yield data for the parameters that resulted in the best quality FG for each feedstock. Values for all pulses are shown in Table S1, Supporting Information.

amorphous (Figure 2a). FJH at 150 V for 500 ms results in AmoC FG (1), with a FG purity of 91% (Figure 2b). AmoC FG (2) is representative of FG made from AmoC using a voltage of 175 V, rather than 150 V in the case of AmoC FG (1). FG purity was calculated by using Raman mapping to obtain at least 100 spectra for each sample and determine what percentage of spectra met the following criteria: 1) a minimum I_{2D}/I_G ratio of ≥ 0.3 , 2) a signal-to-noise ratio of >5 in the 2D band region, and 3) a 2D band with a FWHM of $<100 \text{ cm}^{-1}$. AmoC FG (1) has an I_D/I_G and I_{2D}/I_G ratio of 0.84 and 0.55, respectively, indicating that the AmoC is converted into FG. Process yield for this sample, defined as the mass of product versus the mass of reactant, is $\approx 70\%$.

To effectively convert waste plastic into FG, the waste feedstock must first be made conductive, normally through addition

of a conductive additive, such as carbon black. Instead of carbon black, a 50:50 blend of AmoC:PE was flashed at 200 V for 500 ms (Figure 2c, 50:50 AmoC:PE FG (3)). This results in graphene with a FG purity, I_D/I_G , and I_{2D}/I_G ratios of 99%, 0.513, and 0.721, respectively. Process yield for this material is $\approx 50\%$ due to volatile loss from plastics.^[11] Finally, a 25:75 blend of AmoC:PE was flashed at 150 V for 500 ms, resulting in graphene with a FG purity, I_D/I_G , and I_{2D}/I_G ratios of 93%, 0.50, and 0.60, respectively (Figure 2d, 25:75 AmoC:PE FG (1)). Process yield for this blend is $\approx 40\%$. These results demonstrate that AmoC can be used as a feedstock and as a conductive additive to waste plastic to synthesize high-quality FG. Current as a function of pulse time and yield data for each set of FJH parameters is shown in Figure 2e and Table S1, Supporting Information.

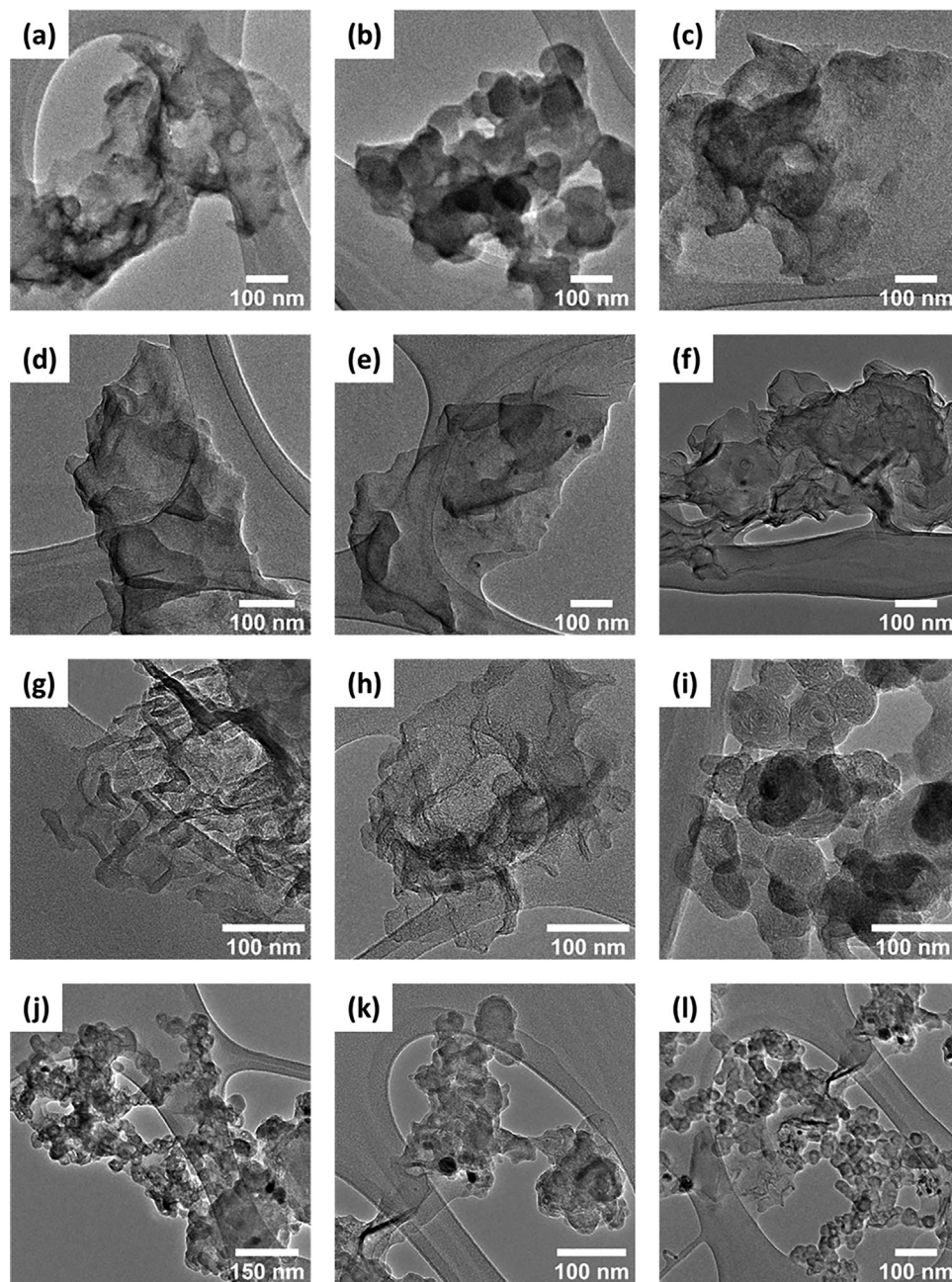


Figure 3. TEM images of a–c) AmoC, d–f) AmoC FG, g–i) 50:50 AmoC:PE FG, and j–l) 25:75 AmoC:PE FG.

Transmission electron microscopy (TEM) is also valuable for analyzing the morphology of carbon materials. Images of the AmoC feedstock reveals that the material is amorphous with very little order (Figure 3a–c). Upon FJH, the AmoC feedstock is converted into large flakes of FG with lateral flakes sizes >500 nm (Figure 3d–f). FJH of a 50:50 blend of AmoC:PE reveals that these large flakes are present (Figure 3g–i), as well as small flakes (≈ 30 to 80 nm) that are typically observed in waste-plastic derived FG.^[11] As the proportion of PE increases, so does the concentration of small flakes in the material, as observed in images of the 25:75 AmoC:PE blend (Figure 3j–l).

Scanning electron microscopy (SEM) is another valuable tool for analyzing the morphology of carbon materials. Images of the AmoC feedstock reveal that the AmoC is indeed amorphous, as evidenced by the lack of order (Figure 4a–c). Upon conversion of AmoC, large particles of AmoC FG are observed (Figure 4d–f). Finally, conversion of the 50:50 and 25:75 AmoC:PE blends results in both large and small particles, which result from the AmoC and the PE feedstocks, respectively (Figure 4g–l).

Addition of 5 wt% of any type of FG, including AmoC FG, 50:50 AmoC:PE FG, and 25:75 AmoC:PE FG results in an increase in Young's modulus and hardness, compared to neat VE

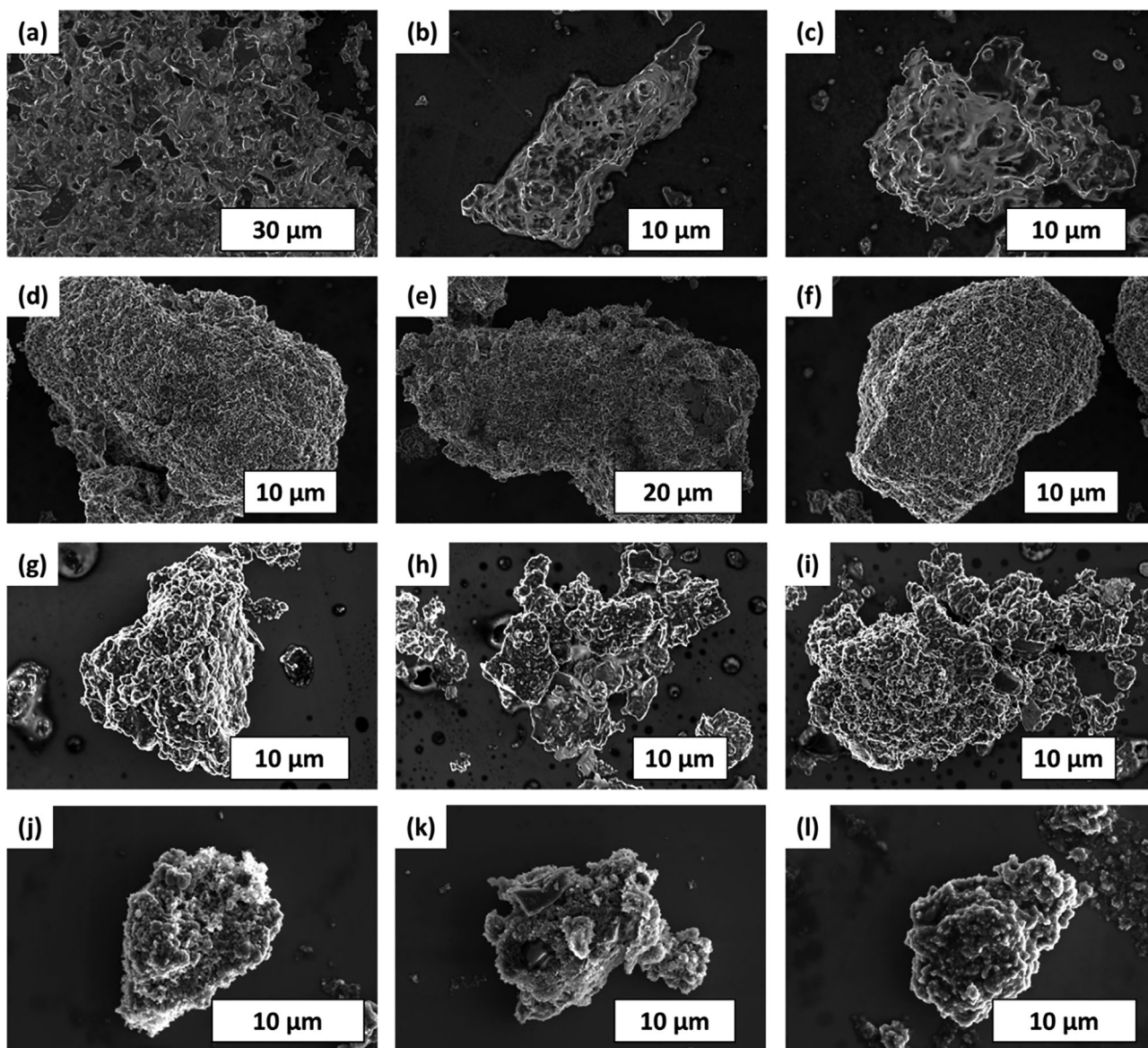


Figure 4. SEM images of a–c) AmoC, d–f) AmoC FG, g–i) 50:50 AmoC:PE FG, and j–l) 25:75 AmoC:PE FG.

(Figure 5a). 5 wt% of AmoC FG grants the greatest increase in Young's modulus of 49%. 5 wt% of 50:50 AmoC:PE FG grants the greatest increase in hardness of 69%. Increasing the wt% loading of 50:50 AmoC:PE FG in VE results in greater gains to the Young's modulus, with comparable hardness to each other (Figure 5b). A table with all values can be found in Table S2, Supporting Information.

Addition of FG can also improve the mechanical properties of DGEBA. AmoC FG improves the Young's modulus by 35% and hardness by 73% at 5 and 3 wt% loading, respectively (Figure 5c). FG made from a 50:50 blend of AmoC:PE improves the Young's modulus by 60% and hardness by 59% at 1 and 3 wt% loading, respectively (Figure 5d). 25:75 AmoC:PE FG improves the Young's modulus by 73% and hardness by 65% at 1 wt% loading (Figure 5e). A table with all values can be found in Table S3, Supporting Information. Greater improvement in mechanical prop-

erties can be observed with FG made from a blend of AmoC and PE, likely due to the range of sizes present in the additive. As loadings of FG exceed an optimum concentration, a gradual decrease in the enhancement of mechanical properties is observed, likely due to weak interfacial interactions between the FG and the matrix material. The samples were found to be non-conductive after testing with a multimeter, likely because the level of dispersion needed for conductivity in this high-viscosity system is difficult to achieve with mechanical methods, as shown here. Should conductivity be desired, an alternative mixing method, such as solution mixing, is likely necessary.

Life cycle assessments were prepared comparing the environmental impacts of neat VE or DGEBA against composites with varying loadings of AmoC FG (Figure S2 and Table S4, Supporting Information), 50:50 AmoC:PE FG (Figure S3 and Table S5, Supporting Information), and 25:75 AmoC:PE FG (Figure S4 and

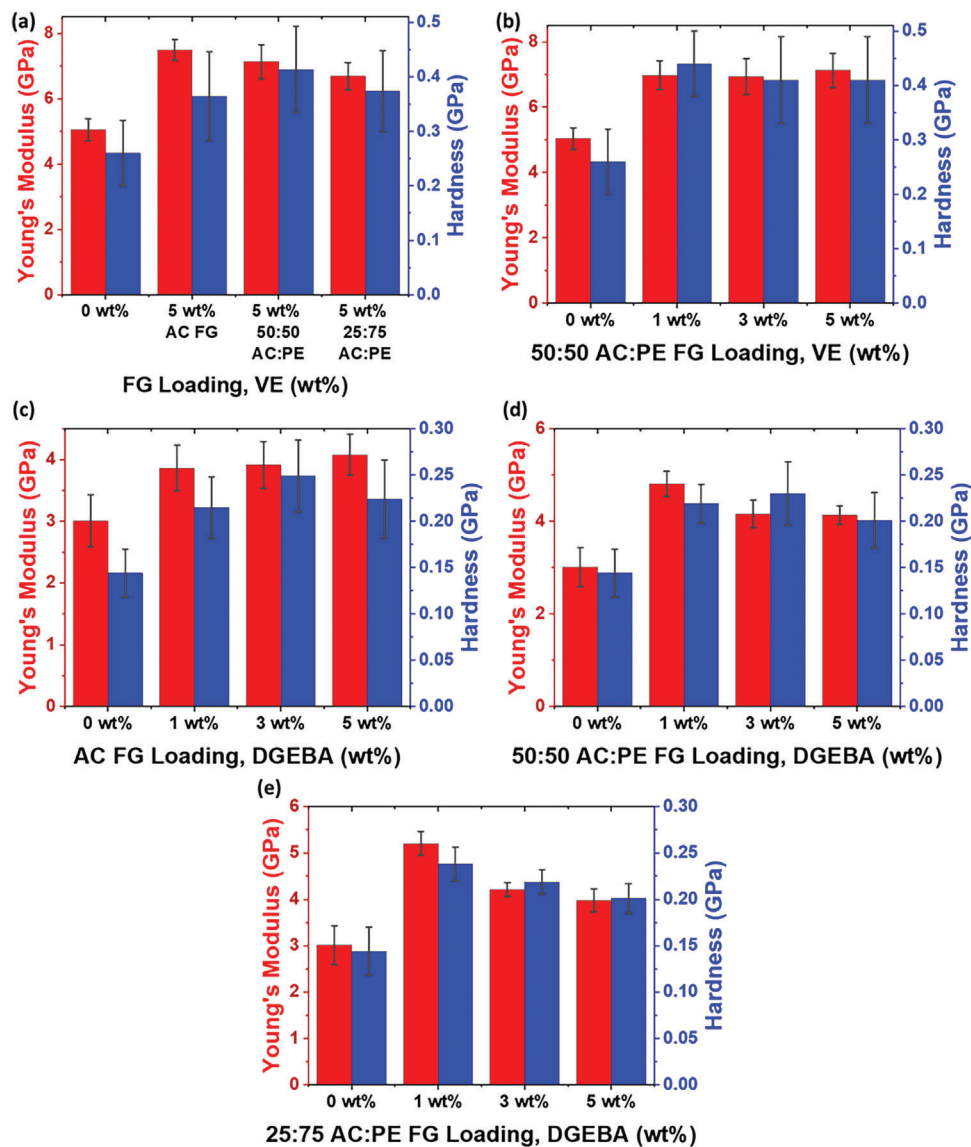


Figure 5. Mechanical testing of VE and DGEBA composites with FG additives. Here, Amoc is replaced by AC for brevity. Comparison of mechanical properties of a) neat VE and 5 wt% loadings of FG made from varying feedstocks. Mechanical properties of b) neat VE and varying wt% loadings of 50:50 AC:PE FG. Mechanical properties of neat DGEBA and varying wt% loadings of c) AC FG, d) 50:50 AC:PE FG, and e) 25:75 AC:PE FG.

Table S6, Supporting Information). 1 metric ton is used as the functional unit (Figure 6a–c). The data used for calculating the input and output of processes including epoxy production, removal of waste PE, Amoc production, and electricity usage for the FJH process were based on literature.^[32] Saratoga Energy reports that 3.76 kg of CO₂ are consumed for each kg of Amoc that is produced. Key assumptions include the use of U.S. Central and Southern Plains Mix of electricity and that the PE used in production of Amoc:PE FG would otherwise be incinerated as fuel. Material transportation and waste stream disposal/remediation were defined as being outside the scope of this contribution. Background data was sourced primarily from Argonne National Laboratory's GREET model including GREET.Net software and spreadsheet models.

Addition of 5 wt% Amoc FG to VE results in 6.8% and 5.1% decreases in CO₂ emissions and water consumption, respectively. However, this results in a 0.3% increase in energy consumption, due to the energetic cost associated with molten carbonate electrolysis for conversion of CO₂ to amorphous carbon. Addition of 5 wt% 50:50 Amoc:PE FG to VE results in a 7.6%, 5%, and 1.3% decrease in CO₂ emissions, water consumption, and energy consumption, respectively. Addition of 5 wt% 25:75 Amoc:PE FG to VE results in a 7.7%, 5%, and 2.7% decrease in CO₂ emissions, water consumption, and energy consumption, respectively. As such, we can demonstrate that use of FG made from Amoc and Amoc:PE improves the mechanical properties of VE and DGEBA at low strains, while also reducing the environmental impacts of using such materials.

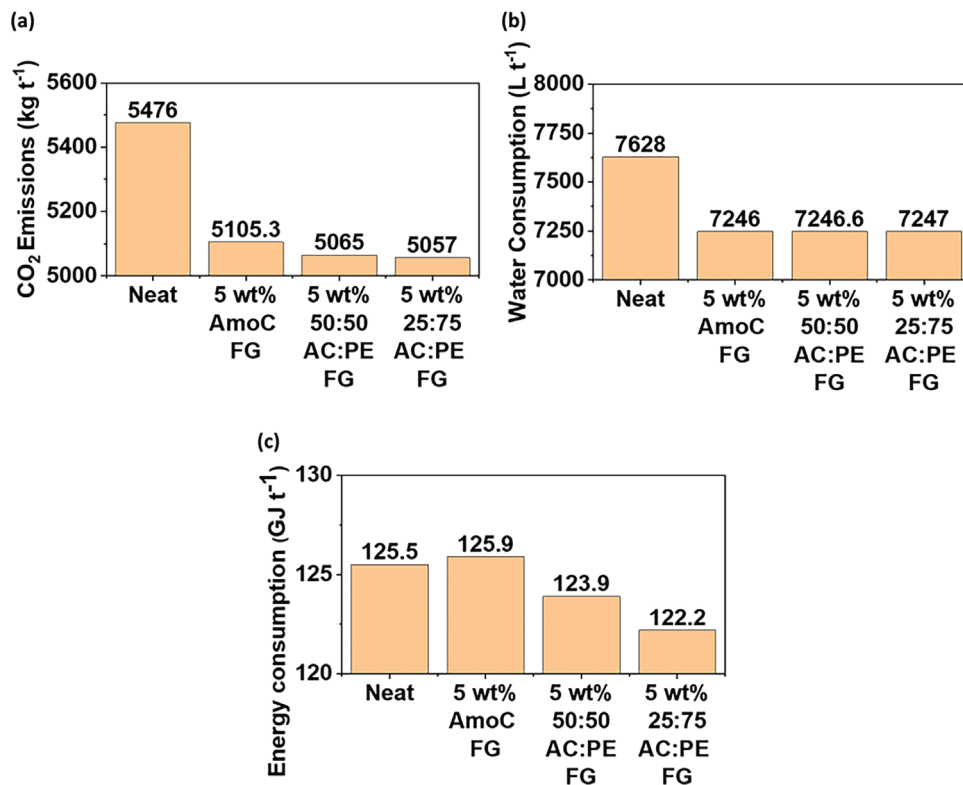


Figure 6. Life cycle assessment comparison of a) CO₂ emissions, b) water consumption, and c) energy consumption of neat VE or DGEBA and composites made with 5 wt% loadings of different types of FG. Here, AmoC is used interchangeably with AC for brevity.

Macroscale compressive testing of neat VE and VE with 50:50 AmoC:PE FG shows that the Young's modulus of VE with FG is comparable or higher than the neat materials (Figure S5, Supporting Information). However, the yield strength and yield strain of the neat VE is higher. This occurs when nanofillers do not have good interfacial interactions with the matrix material. Without this interaction, Van der Waals forces are enough to bind the fillers to the matrix and transfer stress between the materials, resulting in the increased modulus at small strains, such as those measured with triboindentation. At high strains, these composite materials yield at lower stresses and strains.

The interfacial interactions between graphene and the polymer matrix can be improved by maximizing the contact surface area through various preparation methods and by functionalizing the surface of the graphene. Several methods, including solution blending, melt blending, and in situ polymerization, have been shown to maximize the contact interface by evenly dispersing graphene in the polymer matrix.^[33,34] In this contribution, a form of in situ polymerization is used, but the viability of other preparation methods is not yet investigated.

Covalent and non-covalent functionalization can also be used to enhance the interfacial interactions between graphene and the polymer matrix.^[35,36] The C=C bond can be used to perform a variety of covalent functionalization reactions, albeit at the cost of π -conjugation. Non-covalent functionalization maintains the bulk structure and specific properties of graphene but require new solvents or surfactants to be introduced into the system.

3. Conclusion

Here, amorphous carbon derived from CO₂ through molten carbonate electrolysis is converted into FG both on its own and blended with PE in varying ratios. Conversion of these feedstocks is confirmed through SEM, TEM, and Raman spectroscopy. The FG products are then used as a reinforcing additive in VE with a maximum increase in Young's modulus and hardness of 49% and 69%, respectively, with different loadings under triboindentation. The same additives can be used in DGEBA with a maximum increase in Young's modulus and hardness of 73% and 73%, respectively. Life cycle assessment also shows that adding 5 wt% 25:75 AmoC:PE FG to the matrix material results in 7.7%, 5%, and 2.7% decreases in CO₂ emissions, water consumption, and energy consumption, respectively. However, a lack of sufficient interaction between the FG and the VE means that at higher strains, neat VE possesses higher yield strength and yield strain than the AmoC FG:VE composites. As such, while we demonstrate the preparation and use of a CO₂-negative reinforcing additive derived from CO₂ and waste plastic, further optimization of the filler/matrix match is required.

4. Experimental Section

Materials: Vinyl ester resin (VE, RS-392-2248-40 vinylester laminating resin) and MEKP were obtained from Fiberglass Supply Depot (Fort Pierce, FL) and used as received. AmoC was obtained from Saratoga Energy and used as received. According to Saratoga Energy's reports,

it requires 40 kWh to produce 1 kg of AmoC. Polyethylene (PE) waste was obtained by shredding high density PE milk jugs into particles with average sizes ≈ 1 mm using a Shanghai Ke Heng Industrial Co. cutter. DGEBA was obtained from Millipore-Sigma (Lot: MKCK4566) and used as received. A curing agent, 1,5-diamino-2-methylpentane, was also obtained from Millipore-Sigma (Lot #: SHBG9920V) and used as received.

Flash Joule Heating: AmoC and blends of AmoC:PE were packed between two copper electrodes with copper wool spacers contained within quartz tubes. These tubes were 5 mm long and 2 mm thick with inner and outer diameters of 8 and 12 mm, respectively.^[13] The electrodes were machined such that they fit loosely into the quartz tube to permit outgassing. Samples of AmoC were compressed to obtain resistances of 1.8–1.9 Ω for a weight of 100 mg prior to DC FJH. AmoC on its own was conductive enough to carry out FJH. Shredded PE was not conductive enough for FJH, even when mixed with 25% AmoC and 75% PE. When AmoC was used with PE, an additional AC heating step was needed to carbonize the plastic, making the PE conductive enough for FJH. All carbon sources other than graphite can be used as feedstocks for FJH, however, some samples require a carbon additive to lower resistivity. Samples of 50:50 AmoC:PE and 25:75 AmoC:PE with a weight of 500 mg were compressed to obtain resistances of $< 100 \Omega$ prior to AC FJH (120 V, 60 Hz). The samples were treated for 5 s using AC FJH in a vacuum desiccator (100 mm Hg) to facilitate outgassing of volatile materials, similar to a process that was formerly described.^[11] Afterward, DC FJH was carried out on all samples using a capacitor bank with ten capacitors of 450 V and 640 mF. Exact pulse voltages and pulse times are shown in Table S1, Supporting Information.

Conventional carbonization^[37] requires a high-temperature heat-treatment process in oxidative or inert atmospheres under atmospheric or high pressure. The process can be carried out in the absence or presence of catalysis. As such, conventional carbonization likely requires a greater amount of energy to carry out than AC FJH, given that a furnace needs to be heated to a high temperature under controlled conditions for a long period of time. Hence, the authors consider it to be more energy efficient to use AC FJH rather than conventional carbonization to carbonize the PE material used for FJH.

Composite Preparation: VE composites were prepared by combing ≈ 4.5 g of VE with the desired wt% loading of FG additive in a 20 mL scintillation vial. The solution was mixed using a magnetic stir bar for 30 min at 300 rpm. After stirring, the solution was then shear mixed with a homogenizer obtained from Cole–Parmer (Tissue Tearor 986370-07 Homogenizer; 120 VAC, 1.2 A) for 5 min at $\approx 10\,000$ rpm. A weight of MEKP equal to $\approx 1.5\%$ of the weight of VE was then added to the solution while stirring with a magnetic stir bar at 300 rpm for 5 min and the stir bar was then removed. The solution was then allowed to cure in the scintillation vial overnight. The vial was then broken, and the composite was extracted for sanding with an abrasive wheel. Sandpapers with increasing grits of 100, 800, 1000, 1200, 2000, 2500, and 3000 were used to remove the remaining glass and shape the composite to the appropriate dimensions for mechanical testing.

DGEBA composites were prepared by combining 3.0 g of DGEBA with 0.45 g of 1,5-diamino-2-methylpentane in a 20 mL scintillation vial. Stir bar mixing and shear mixing were carried out as previously described. The slurry was then degassed in a vacuum desiccator for 2 h to remove air bubbles. Afterward, the composite was cured on a hot plate for 2 h at $\approx 70^\circ\text{C}$ before curing at room temperature overnight. The composite was released from the vial and sanded as previously described.

Raman Spectroscopy: Raman spectra were collected with a Renishaw inVia confocal Raman microscope and a 532 nm laser. A 50 \times objective lens was used with a laser power of 5 mW to scan the samples from 1300–2800 cm^{-1} . Large-area Raman mapping was used to determine the crystallinity and morphology of the graphene before analysis of the spectra with a custom-written Python script using the RamPy package. Collected spectra were background-corrected and a Savitsky–Golay filter was used to smooth the spectra before quantification of graphene yield and peak ratios. To qualify as graphene, three criteria were used to assess individual spectra: 1) a minimum I_{2D}/I_G ratio of ≥ 0.3 , 2) a signal-to-noise ratio of > 5 in the 2D band region, and 3) a 2D band with a FWHM of $< 100 \text{ cm}^{-1}$.

Triboindentation: Nanoindentation was carried out using a Hysitron TI 980 Triboindenter equipped with a Berkovich tip with a pyramidal geometry. To calculate the indentation modulus and hardness of VE composites, ten different indentations were performed for each sample with a maximum displacement of 100 nm and a displacement rate of 10 nm s^{-1} . The tip was held steady at the maximum displacement for 10 s to account for creep. Elastic modulus and hardness were calculated using the Oliver–Pharr approach, employing Equations (1)–(3).^[38,39]

$$E_r = \frac{\sqrt{\pi}}{2} \frac{S}{\sqrt{A_p}} \quad (1)$$

$$\frac{1}{E_r} = \frac{1 - \nu^2}{E} + \frac{1 - \nu_i^2}{E_i} \quad (2)$$

$$H = \frac{P}{A_p} \quad (3)$$

where E_r is the reduced elastic modulus; S is the stiffness of the initial part of the unloading curve; A_p is the projected area of contact; E and ν are the elastic modulus and Poisson's ratio of the sample, respectively; E_i and ν_i are the elastic modulus and Poisson's ratio of the indenter, respectively; H is the hardness; and finally, P is the applied load. DGEBA composites were measured with five different indentations with a maximum displacement of 1000 nm and a displacement rate of 10 nm s^{-1} .

Compressive Testing: Stress–strain curves were obtained through uniaxial compressive tests at room temperature with a standard compressive testing machine (Instron 4505). Samples of varying thickness (8–10 mm) and similar diameter (≈ 25 mm) were held between two cross-heads, checked to avoid misalignment, and then compressed at a constant rate of 2 mm min^{-1} . Three samples of each loading of FG in VE were tested to ensure consistency of the results. Strain was calculated based on the individual thickness of each sample, given the varying thicknesses.

TEM: Dilute solutions ($\approx 1 \text{ mg mL}^{-1}$) of FG in ethanol were cup-horn sonicated for 15 min prior to drop-casting onto a 200 mesh Cu grid with lacey carbon film. A JEOL 2100F field-emission gun TEM at 200 kV was used to image the sample.

SEM: The same dilute solutions in ethanol as above were drop cast onto silicon wafers on a hot plate at $\approx 70^\circ\text{C}$ to remove the ethanol. The SEM images were then obtained with a FEI Helios NanoLab 660 DualBeam SEM system at 5.00 kV with a current of 0.1 nA.

Supporting Information

Supporting Information is available from the Wiley Online Library or from the author.

Acknowledgements

The Air Force Office of Scientific Research (FA9550-22-1-0526) and the U.S. Army Corps of Engineers, ERDC (W912HZ-21-2-0050) funded this work. J.L.B. acknowledges support from the NSF Graduate Research Fellowship Program.

Conflict of Interest

The authors declare the following competing financial interest(s): Rice University owns intellectual property on the synthesis and use of FG. That intellectual property has been licensed to a company in which J.M.T. is a stockholder, but not an officer, director, or employee. Conflicts of interest are mitigated through regular disclosure to and compliance with the Rice University Office of Sponsored Programs and Research Compliance. The authors declare no other conflict of interest.

Data Availability Statement

The data that support the findings of this study are available in the supplementary material of this article.

Keywords

carbon dioxide, conversion, flash graphene, flash Joule heating, waste plastic

Received: July 26, 2023
Revised: September 22, 2023
Published online:

- [1] S. Pacala, R. Socolow, *Science* **2004**, *305*, 968.
- [2] IEA, World Energy Outlook 2007: China and India Insights (accessed: December 2022) <https://iea.blob.core.windows.net/assets/86acf56d-d8cc-4b73-b560-259f061264ad/WorldEnergyOutlook2007.pdf>.
- [3] R. S. Haszeldine, *Science* **2009**, *325*, 1647.
- [4] M. Coyne, V. Smill, R. A. Streatfield, Enriching the Earth: Fritz Haber, Carl Bosch, and the Transformation of World Food Production. *Electron. Green J.* The MIT Press, Cambridge, Massachusetts **2002**. <https://doi.org/10.1215/00021482-79.3.383>.
- [5] C. Liang, Y. Chen, M. Wu, K. Wang, W. Zhang, Y. Gan, H. Huang, J. Chen, Y. Xia, J. Zhang, S. Zheng, H. Pan, *Nat. Commun.* **2021**, *12*, 119.
- [6] S. Wickramasinghe, J. Wang, B. Morsi, B. Li, *Energy Fuels* **2021**, *35*, 11820.
- [7] X. Liu, X. Wang, G. Licht, S. Licht, *J. CO₂ Util.* **2020**, *36*, 288.
- [8] S. Licht, *J. CO₂ Util.* **2017**, *18*, 378.
- [9] J. Ren, A. Yu, P. Peng, M. Lefler, F.-F. Li, S. Licht, *Acc. Chem. Res.* **2019**, *52*, 3177.
- [10] M. Johnson, J. Ren, M. Lefler, G. Licht, J. Vicini, X. Liu, S. Licht, *Mater. Today Energy* **2017**, *5*, 230.
- [11] W. A. Algozeeb, P. E. Savas, D. X. Luong, W. Chen, C. Kittrell, M. Bhat, R. Shahsavari, J. M. Tour, *ACS Nano* **2020**, *14*, 15595.
- [12] X.-Y. Wang, A. Narita, K. Müllen, *Nat. Rev. Chem.* **2018**, *2*, 0100.
- [13] D. X. Luong, K. V. Bets, W. A. Algozeeb, M. G. Stanford, C. Kittrell, W. Chen, R. V. Salvatierra, M. Ren, E. A. Mchugh, P. A. Advincula, Z. Wang, M. Bhatt, H. Guo, V. Mancevski, R. Shahsavari, B. I. Yakobson, J. M. Tour, *Nature* **2020**, *577*, 647.
- [14] M. G. Stanford, K. V. Bets, D. X. Luong, P. A. Advincula, W. Chen, J. T. Li, Z. Wang, E. A. Mchugh, W. A. Algozeeb, B. I. Yakobson, J. M. Tour, *ACS Nano* **2020**, *14*, 13691.
- [15] P. A. Advincula, A. C. De Leon, B. J. Rodier, J. Kwon, R. C. Advincula, E. B. Pentzer, *J. Mater. Chem. A* **2018**, *6*, 2461.
- [16] P. A. Advincula, D. X. Luong, W. Chen, S. Raghuraman, R. Shahsavari, J. M. Tour, *Carbon* **2021**, *178*, 649.
- [17] J. L. Beckham, K. M. Wyss, Y. Xie, E. A. Mchugh, J. T. Li, P. A. Advincula, W. Chen, J. Lin, J. M. Tour, *Adv. Mater.* **2022**, *34*, 2106506.
- [18] P. A. Advincula, V. Granja, K. M. Wyss, W. A. Algozeeb, W. Chen, J. L. Beckham, D. X. Luong, C. F. Higgs III, J. M. Tour, *Carbon* **2022**, *203*, 876.
- [19] M. A. S. R. Saadi, P. A. Advincula, M. S. H. Thakur, A. Z. Khater, S. Saad, A. Shayesteh Zeraati, S. K. Nabil, A. Zinke, S. Roy, M. Lou, S. N. Bheemasetti, M. A. A. Bari, Y. Zheng, J. L. Beckham, V. Gadhamshetty, A. Vashisth, M. G. Kibria, J. M. Tour, P. M. Ajayan, M. M. Rahman, *Sci. Adv.* **2022**, *8*, eadd3555.
- [20] W. Chen, J. T. Li, Z. Wang, W. A. Algozeeb, D. X. Luong, C. Kittrell, E. A. Mchugh, P. A. Advincula, K. M. Wyss, J. L. Beckham, M. G. Stanford, B. Jiang, J. M. Tour, *ACS Nano* **2021**, *15*, 11158.
- [21] W. Chen, J. T. Li, C. Ge, Z. Yuan, W. A. Algozeeb, P. A. Advincula, G. Gao, J. Chen, K. Ling, C. H. Choi, E. A. Mchugh, K. M. Wyss, D. X. Luong, Z. Wang, Y. Han, J. M. Tour, *Adv. Mater.* **2022**, *34*, 2202666.
- [22] W. Chen, C. Ge, J. T. Li, J. L. Beckham, Z. Yuan, K. M. Wyss, P. A. Advincula, L. Eddy, C. Kittrell, J. Chen, D. X. Luong, R. A. Carter, J. M. Tour, *ACS Nano* **2022**, *16*, 6646.
- [23] S. J. Barnes, *Environ. Pollut.* **2019**, *249*, 812.
- [24] J. Zheng, S. Suh, *Nat. Clim. Chang.* **2019**, *9*, 374.
- [25] W. E. Forum, The New Plastics Economy: Rethinking the Future of Plastics (accessed: November 2022) https://www3.weforum.org/docs/WEF_The_New_Plastics_Economy.pdf.
- [26] J. C. Prata, *Environ. Pollut.* **2018**, *234*, 115.
- [27] K. D. Cox, G. A. Covernton, H. L. Davies, J. F. Dower, F. Juanes, S. E. Dudas, *Environ. Sci. Technol.* **2019**, *53*, 7068.
- [28] M. Shen, S. Ye, G. Zeng, Y. Zhang, L. Xing, W. Tang, X. Wen, S. Liu, *Mar. Pollut. Bull.* **2020**, *150*, 110712.
- [29] K. Kvale, A. E. F. Prowe, C.-T. Chien, A. Landolfi, A. Oschlies, *Nat. Commun.* **2021**, *12*, 2358.
- [30] S. Sharma, S. Chatterjee, *Environ. Sci. Pollut. Res.* **2017**, *24*, 21530.
- [31] NOAA, How much oxygen comes from the ocean? (accessed: July 2022) <https://oceanservice.noaa.gov/facts/ocean-oxygen.html#:~:text=Scientists%20estimate%20that%20roughly%20half,some%20bacteria%20that%20can%20photosynthesize>.
- [32] G. Keoleian, S. Miller, R. De Kleine, A. Fang, J. Mosley, **2012**, *1*.
- [33] W. Chen, H. Weimin, D. Li, S. Chen, Z. Dai, *Sci. Eng. Compos. Mater.* **2018**, *25*, 1059.
- [34] D. Galpaya, M. Wang, M. Liu, N. Motta, E. Waclawik, C. Yan, *Graphene* **2012**, *01*, 30.
- [35] S. J. Lee, S. J. Yoon, I.-Y. Jeon, *Polymers* **2022**, *14*, 4733.
- [36] R. Atif, F. Inam, *Graphene* **2016**, *05*, 96.
- [37] S. Chen, Z. Liu, S. Jiang, H. Hou, *Sci. Total Environ.* **2020**, *710*, 136250.
- [38] W. C. Oliver, G. M. Pharr, *J. Mater. Res.* **1992**, *7*, 1564.
- [39] X. Han, T. Wang, P. S. Owuor, S. H. Hwang, C. Wang, J. Sha, L. Shen, J. Yoon, W. Wang, R. V. Salvatierra, P. M. Ajayan, R. Shahsavari, J. Lou, Y. Zhao, J. M. Tour, *ACS Nano* **2018**, *12*, 11219.